

# Observations of the low-luminosity Type Iax supernova 2019gsc: a fainter clone of SN 2008ha?\*

Lina Tomasella,<sup>1†</sup> Maximilian Stritzinger,<sup>2</sup> Stefano Benetti,<sup>1</sup> Nancy Elias-Rosa,<sup>1,3</sup> Enrico Cappellaro,<sup>1</sup> Erkki Kankare,<sup>4</sup> Peter Lundqvist,<sup>5,6</sup> Mark Magee,<sup>7</sup> Kate Maguire,<sup>8</sup> Andrea Pastorello,<sup>1</sup> Simon Prentice,<sup>8</sup> Andrea Reguitti,<sup>1</sup>

<sup>1</sup>INAF Osservatorio Astronomico di Padova, Vicolo dell'Osservatorio 5, 35122 Padova, Italy

<sup>2</sup>Department of Physics and Astronomy, Aarhus University, Ny Munkegade 120, DK-8000 Aarhus C, Denmark

<sup>3</sup>Institute of Space Sciences (ICE, CSIC), Campus UAB, Carrer de Can Magrans s/n, 08193 Barcelona, Spain

<sup>4</sup>Tuorla Observatory, Department of Physics and Astronomy, University of Turku, FI-20014 Turku, Finland

<sup>5</sup>Department of Astronomy, AlbaNova University Center, Stockholm University, SE-10691 Stockholm, Sweden

<sup>6</sup>The Oskar Klein Centre, AlbaNova, SE-10691 Stockholm, Sweden

<sup>7</sup>Astrophysics Research Centre, School of Mathematics and Physics, Queen's University Belfast, Belfast BT7 1NN, UK

<sup>8</sup>School of Physics, Trinity College Dublin, Dublin 2, Ireland

Submitted MNRAS

## ABSTRACT

We present optical photometric and spectroscopic observations of the faint-and-fast evolving type Iax SN 2019gsc, extending from the time of  $g$ -band maximum until about fifty days post maximum, when the object faded to an apparent  $r$ -band magnitude of  $m_r \approx 22$ . SN 2019gsc reached a peak luminosity of only  $M_g = -13.68 \pm 0.22$  mag, and is characterised with a post-maximum decline rate  $\Delta m_{15}(g) = 1.66 \pm 0.15$  mag. These light curve parameters are similar to those measured for SN 2008ha of  $M_g = -14.01 \pm 0.14$  mag at peak and  $\Delta m_{15}(g) = 1.80 \pm 0.03$  mag. The spectral features of SN 2019gsc also resemble those of SN 2008ha at similar phases. This includes both the extremely low ejecta velocity at maximum,  $\sim 3,000$  km s<sup>-1</sup>, and at late-time (phase +52 d) strong forbidden iron, nickel and cobalt lines as well as both forbidden and permitted calcium features. Furthermore, akin to SN 2008ha, the bolometric light curve of SN 2019gsc is consistent with the production of  $\approx 0.003 \pm 0.001$  M<sub>⊙</sub> of <sup>56</sup>Ni. The explosion parameters,  $M_{ej} \approx 0.13$  M<sub>⊙</sub> and  $E_k \approx 12 \times 10^{48}$  erg, are also similar to those inferred for SN 2008ha. We estimate a slightly sub-solar oxygen abundance for the host galaxy of SN 2019gsc, ( $12 + \log_{10}(\text{O}/\text{H}) = 8.10 \pm 0.18$  dex), consistent with the equally metal-poor environment of SN 2008ha. Altogether, our dataset of SN 2019gsc indicates that it is a member of a small but growing group of extreme SN Iax that include SN 2008ha and SN 2010ae.

**Key words:** supernovae: general – supernovae: individual: SN 2019gsc (ATLAS19mbg, PS19bex, ZTF19aawhlc)

## 1 INTRODUCTION

Type Iax supernovae (hereafter SNe Iax), also known as 2002cx-like SNe after their prototype described by Li et

al. (2003), are possibly a class of thermonuclear explosions showing some spectroscopic similarities to SNe Ia near maximum light, while at late-time they appear significantly different (e.g., Foley et al. 2016; Jha 2017). In fact, around maximum-light SNe Iax exhibit high-ionization features of Fe II and Fe III, closely resembling the luminous 1991T-like SNe at similar phases. However, their late spectra are dominated by prevalent Ca II permitted and forbidden spectral features in complete contrast to SNe Ia that are instead dominated by broad, forbidden [Fe II] and [Fe III] emission

\* This paper includes data gathered with the 2.56-m Nordic Optical Telescope, the 10.4-m Gran Telescopio Canarias and the Liverpool Telescope located at the Observatorio del Roque de los Muchachos, La Palma, Spain. It also includes data obtained with Las Cumbres Observatory global network.

† E-mail: lina.tomasella@inaf.it

features. Interestingly, the energetics of SNe Iax explosions and their luminosities can be very different from one event to the other: within the class, peak absolute magnitudes range from  $M_{peak} \approx -13$  mag for the fainter members to  $M_{peak} \approx -19$  mag for the brighter ones (the latter close to the peak luminosity of normal SNe Ia; cf. [Jha 2017](#), see his Table 1). In all cases, SNe Iax show maximum-light expansion velocities measured from the Si II  $\lambda 6355$  line that are much lower than those measured in SNe Ia. Quantitatively, at maximum the expansion velocities in SNe Ia are typically of around  $\sim 10,000$  km s<sup>-1</sup>, while the velocities inferred from SNe Iax never exceed 7,000 km s<sup>-1</sup>, and can be as low as 2,000 km s<sup>-1</sup>.

The peculiarities of SNe Iax are challenging the carbon-oxygen (C/O) Chandrasekhar-mass ( $M_{Ch}$ ) white dwarf (WD) explosion channel scenario, which has been the standard paradigm for normal, thermonuclear SNe Ia, including extreme sub-types, such as the luminous 1991T-like and the sub-luminous 1991bg-like SNe Ia (see, e.g., [Taubenberger 2017](#)). A number of alternatives have been proposed to account for the origins of SNe Iax (see the review by [Jha 2017](#)). One popular scenario consists of a carbon-oxygen or a carbon-oxygen-neon WD that accretes helium from a He-star companion, explodes upon reaching the Chandrasekhar limit, yet does not fully disrupt and thereby leaves a bound remnant ([Liu et al. 2010](#); [Jordan et al. 2012](#); [Kromer et al. 2013, 2015](#)). Such failed deflagrations may explain relatively bright but low ejecta velocity events such as SN 2014ck ([Tomasella et al. 2016](#)), while the scenario does have difficulties to explain observations of the brightest type Iax members such as SN 2012Z (see, e.g., [Stritzinger et al. 2015](#)). [McCully et al. \(2014\)](#) reported a plausible progenitor detection in pre-explosion *Hubble Space Telescope* (HST) images, consisting of a blue source similar to the Galactic helium nova V445-Pup at the location of SN 2012Z. Further HST imaging of the SN 2012Z in the years after explosion also reveals a source at its position ([McCully et al. 2014](#)), however it is not clear if this source is a bound remnant, or the companion star. In order to test the various models proposed for SN Iax a larger observational dataset of SN Iax is needed, especially of the low end of the peak luminosity distribution.

Soon after discovery, [Leloudas et al. \(2019\)](#) provided the spectroscopic classification of SN 2019gsc as a type Iax event. Furthermore, it was noted the peculiar nature of this object, as it closely resembles the type Iax SNe 2008ha and 2010ae ([Foley et al. 2009](#); [Valenti et al. 2009](#); [Stritzinger et al. 2014](#)), the faintest and least-energetic SNe Iax yet observed. The preliminary photometric observations of SN 2019gsc indicated that it could be even fainter than the extreme SN 2008ha.

This paper presents optical spectroscopic and photometric observations of SN 2019gsc that, as we will show, shares many characteristic to both SN 2008ha and SN 2010ae over its entire evolution. This paper is organized as follows: in Section 2 we provide basic information about the SN discovery, its host galaxy, our observations and the data reduction procedures. In Section 3, the photometric evolution and photometric parameters of SN 2019gsc are presented, while the spectroscopic analysis is reported in Section 4. In Section 5 we examine the environment of SN 2019gsc and set in context with that of other faint SNe Iax. Discussion and conclusions are in Section 6.

## 2 DISCOVERY AND FOLLOW-UP OBSERVATIONS OF SN 2019GSC

SN 2019gsc (also known as ATLAS19mbg, PS19bex and ZTF19aawhlcn) was discovered on 2019 June 02.35 UT by the ATLAS (Asteroid Terrestrial-impact Last Alert System) Project ([Tonry 2011](#)), at a cyan-ATLAS AB magnitude of 19.66 (Tonry et al.; TNS Astronomical Transient Report No. 36575). The discovery report also noted a non-detection two days earlier (2019 May 31.39 UT) although in a different filter (orange-ATLAS) and not very deep (19.34 mag). The SN is located in the irregular galaxy SBS 1436+529A (other name: PGC052275), see Fig. 1, which is characterized by the presence of clumpy H II regions, similarly to SN 2008ha's host-galaxy UGG 12682. The galaxy is described as a merger system, with two nuclei separated by 3.8 arcsec, which corresponds to 0.9 kpc ([Huchtmeier et al. 2008](#)).

A heliocentric recessional velocity of  $3384 \pm 3$  km s<sup>-1</sup> for SBS 1436+529A is reported in the NASA/IPAC Extragalactic Database (NED) estimated from the Sloan Digital Sky Survey Data Release 3<sup>1</sup> observations. Adopting  $H_0 = 73.2 \pm 1.7$  km s<sup>-1</sup> Mpc<sup>-1</sup> ([Riess et al. 2016](#)) and corrections for peculiar motions due to influences of the Virgo cluster, the Great Attractor, and the Shapley supercluster ([Mould et al. 2000](#)), we obtain a Hubble flow distance and distance modulus to the host of SN 2019gsc of  $53.4 \pm 3.7$  Mpc and  $\mu = 33.64 \pm 0.15$  mag, respectively.

A spectrum of SN 2019gsc was obtained a day after discovery, on 2019 June 03.97 UT ([Leloudas et al. 2019](#)) with the Nordic Optical Telescope 2.56m (NOT), and it was found very similar to that of SN 2010ae ([Stritzinger et al. 2014](#)) at around the maximum light. SN 2019gsc exhibits a number of lines with low velocities, between 2,000–3,500 km s<sup>-1</sup>. In particular, the expansion velocity measured from the Si II  $\lambda$  6355 line is  $\approx 3,500$  km s<sup>-1</sup>.

Given the relatively small number of well-observed SNe Iax in the literature ([Jha 2017](#)) and the close similarity of SN 2019gsc to the faintest members of this peculiar class of likely thermonuclear supernovae, we initiated a follow-up campaign to collect optical spectroscopic and photometric observations. Our follow-up began as soon as SN 2019gsc was classified. However, due to the low-luminosity and rapid evolution, the observing campaign was terminated just 52 d later (see Section 4.1).

The NASA Extragalactic Database (NED) provides a Milky Way reddening in the direction of SBS 1436+529A of  $E(B - V)_{MW} = 0.008 \pm 0.005$  mag ([Schlafly & Finkbeiner 2011](#)). We do not detect interstellar Na I D lines at the redshift of the host, therefore we assume that the reddening in the host of SN 2019gsc is minimal.

Basic information of SN 2019gsc and its host galaxy is summarized in Table 1. The logbook of observations is reported in Tables 2 and 3.

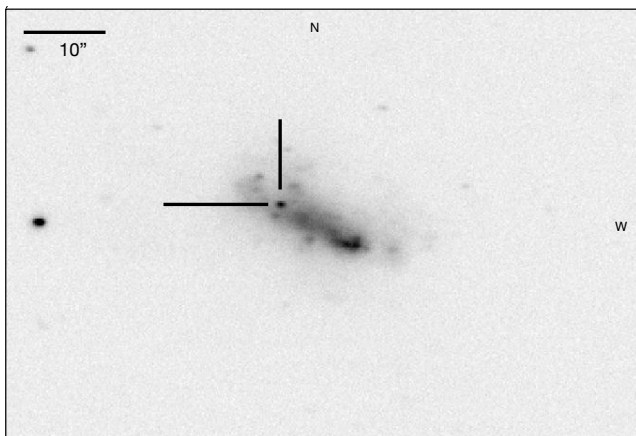
### 2.1 Photometric data reduction

Optical multi-band (*ugriz*) imaging of SN 2019gsc started soon after discovery and continued over the course of about

<sup>1</sup> <http://www.sdss.org/dr3/products/spectra/getspectra.html>

**Table 1.** Basic information on SN 2019gsc and its host-galaxy SBS 1436 + 529A.

Host galaxy	SBS 1436+529A (PGC052275)
Galaxy type	Irregular
Heliocentric radial velocity	$3384 \pm 3 \text{ km s}^{-1}$
Redshift ( $z$ )	0.011288
Distance modulus	$33.64 \pm 0.15 \text{ mag}$
Galactic extinction	$A_B = 0.034 \text{ mag}$ $A_V = 0.026 \text{ mag}$
SN spectral type	Iax
RA (J2000.0)	$14^{\text{h}}37^{\text{m}}45.24^{\text{s}}$
Dec (J2000.0)	$+52^{\circ}43'36.43''$
Discovery date	2019-06-02 08:31:12 UT (ATLAS cyan mag 19.66)
Last no-detection	2019-05-31 09:27:21 UT
Date of g-band maximum	2019-06-03 (MJD 58637)
$m_g$ at maximum	$19.98 \pm 0.20 \text{ mag}$
$M_g$ at maximum	$-13.68 \pm 0.22 \text{ mag}$
$M_r$ at maximum	$-14.25 \pm 0.25 \text{ mag}$
$\Delta m_{15}(g)$	$1.66 \pm 0.15 \text{ mag}$
$L_{\text{bol}}$ at maximum	$8.9 \times 10^{40} \text{ erg}$

**Figure 1.** Finding chart of SBS 1436+529A (PGC052275) constructed with a g-band image obtained with the NOT (+ AL-FOSC) on 2019 June 07. The position of SN 2019gsc is marked.

three weeks, revealing the SN faded by roughly two magnitudes down to  $m_g \sim 22 \text{ mag}$ . The telescopes and instruments used for photometric followup campaign are listed in Table 2.

All science images were pre-processed using standard procedures in IRAF<sup>2</sup> for bias subtraction and flat fielding. The Sloan Digital Sky Survey (SDSS; Data Release 15, Aguado et al. 2019)<sup>3</sup> stars in the field of SBS 1436+529A were used as a local photometric reference.

Accurate photometric measurements of SN 2019gsc requires galaxy subtraction to isolate the SN flux contribution. We therefore used the SDSS images obtained on 2003

March 07 as templates to remove the host-galaxy contamination from each of the *ugriz*-band science images. The final calibrated photometry (cf. Table 2) was derived with the SNOoPY pipeline<sup>4</sup>, using the PSF-fitting technique on the template-subtracted science images and the instrumental magnitudes were then calibrated to the Sloan AB system, using Sloan stars in the field of the host galaxy.

Error estimates for the SN magnitudes are obtained through artificial star experiments in which fake stars with a similar magnitudes as the SN are placed in the fit residual image in a position close to, but not coincident with, the SN location. The simulated images are processed through the same procedure and the standard deviation of the measured magnitudes of the fake stars is taken as an estimate of the instrumental magnitude error. In practical term this errors mainly reflects uncertainty in the background subtraction. The photometry is reported in Table 2 and plotted in Fig. 2.<sup>5</sup>

The early photometric epochs of SN 2019gsc obtained by the Zwicky Transient Factory survey (Kulkarni 2018, ZTF) are also added in our analysis. Data were retrieved from the Transient Name Server (TNS)<sup>6</sup> and Lasair<sup>7</sup> (Smith, et al. 2019), listed in Table 2 and plotted in Fig. 2 as open circles. The cyan- and orange-ATLAS filters are non-standard; so the discovery and non-detection magnitudes mentioned at the beginning of Section 2 are not used in our analysis.

## 2.2 Spectroscopic data reduction

Three low-resolution optical spectra of SN 2019gsc were obtained at phases +1 d, +9 d and +52 d relative to the epoch of g-band maximum (cf. Table 3). The first two of these spectra were obtained with the 2.56-m Nordic Optical Telescope (NOT) via NUTS2 (NOT Un-biased Transient Survey 2) collaboration<sup>8</sup>, and the third one with the 10.4-m Gran Telescopio Canarias (GTC). We used standard procedures and IRAF tasks for the data reduction. After bias and flat-field correction, the SN spectrum was extracted and calibrated in wavelength with reference to standard arc lamp spectra. For the flux calibration, nightly sensitivity functions were derived from observations of spectrophotometric standard stars. Corrections for the telluric absorption bands were also derived using the spectrophotometric standard star spectra. A non-perfect removal of telluric absorption can affect the SN spectra, particularly at the position of the strong O<sub>2</sub> A-band located between 7590–7650 Å. Finally, the flux-calibration of each spectrum was verified against coeval broadband photometry.

<sup>4</sup> SNOoPY is a package for SN photometry through PSF fitting and template subtraction developed by E. Cappellaro. A package description can be found at <http://sngroup.oapd.inaf.it/snoopy.html>

<sup>5</sup> Note that since only five upper limits and two epochs are available for the *u*- and *z*-bands, respectively, their values are listed in Table 2 but not include in Fig. 2.

<sup>6</sup> <https://wis-tns.weizmann.ac.il/>

<sup>7</sup> <https://lasair.roe.ac.uk/object/ZTF19aawhlc/>

<sup>8</sup> <http://csp2.lco.cl/not/>

<sup>2</sup> IRAF was distributed by the National Optical Astronomy Observatory, which is operated by the Association of Universities for Research in Astronomy (AURA) under cooperative agreement with the National Science Foundation.

<sup>3</sup> <https://www.sdss.org/dr15>

**Table 2.** Optical photometry of SN 2019gsc. Sloan *ugriz* filters (ABmag).

Date	MJD	phase <sup>a</sup>	<i>u</i> (mag)	<i>g</i> (mag)	<i>r</i> (mag)	<i>i</i> (mag)	<i>z</i> (mag)	Survey or telescope <sup>b</sup>
<b>Data from <i>Lasair</i>:</b>								
2019-05-25	58628.30	-9	...	...	>20.495	...	...	ZTF
2019-05-25	58628.22	-9	...	>20.617	...	...	...	ZTF
2019-05-29	58632.28	-5	...	...	>20.455	...	...	ZTF
2019-06-01	58635.23	-2	...	19.848 (0.166)	...	...	...	ZTF
2019-06-01	58635.26	-2	...	...	19.933 (0.133)	...	...	ZTF
2019-06-04	58638.20	1	...	19.922 (0.177)	...	...	...	ZTF
2019-06-04	58638.26	1	...	...	19.717 (0.123)	...	...	ZTF
2019-06-07	58641.30	4	...	...	19.737 (0.111)	...	...	ZTF
2019-06-10	58644.20	7	...	20.303 (0.287)	...	...	...	ZTF
2019-06-13	58647.25	11	...	...	19.790 (0.171)	...	...	ZTF
<b>Data from this work:</b>								
2019-06-05	58639.98	2	>19.950	19.970 (0.050)	19.673 (0.054)	19.701 (0.038)	...	LT
2019-06-06	58640.26	4	...	19.955 (0.032)	19.716 (0.050)	19.663 (0.071)	...	LCO
2019-06-08	58642.13	6	...	19.984 (0.029)	19.650 (0.016)	19.658 (0.021)	19.940 (0.047)	NOT
2019-06-08	58642.15	6	...	20.007 (0.049)	19.551 (0.043)	19.671 (0.067)	...	LCO
2019-06-08	58643.00	6	>20.292	20.175 (0.059)	19.578 (0.043)	19.673 (0.035)	...	LT
2019-06-09	58643.35	7	...	20.150 (0.400)	19.553 (0.044)	19.686 (0.073)	...	LCO
2019-06-11	58645.96	9	>20.246	20.561 (0.137)	19.750 (0.061)	19.725 (0.061)	...	LT
2019-06-12	58646.32	10	...	20.472 (0.103)	19.713 (0.076)	19.807 (0.130)	...	LCO
2019-06-15	58649.01	13	>19.283	20.715 (0.066)	20.071 (0.131)	19.863 (0.076)	...	LT
2019-06-16	58650.34	14	...	>21.068	20.151 (0.123)	19.894 (0.139)	...	LCO
2019-06-17	58651.98	15	>19.247	21.124 (0.107)	20.231 (0.144)	20.019 (0.037)	...	LT
2019-06-18	58652.24	16	...	21.140 (0.205)	20.309 (0.173)	19.964 (0.121)	...	LCO
2019-06-20	58654.21	18	...	21.438 (0.185)	20.340 (0.147)	>19.967	...	LCO
2019-06-23	58657.15	21	...	21.718 (0.229)	20.550 (0.208)	>20.264	...	LCO
2019-06-24	58658.31	22	...	22.007 (0.188)	20.779 (0.097)	20.226 (0.080)	...	LCO
2019-07-02	58666.97	30	...	>22.513	>21.896	20.665 (0.029)	20.175 (0.057)	NOT

<sup>a</sup> Phase is relative to the epoch of *g*-band maximum MJD = 58637.

<sup>b</sup> NOT = Nordic Optical Telescope, LT = Liverpool Telescope, LCO = Las Cumbres Observatory global network.

**Table 3.** Log of spectroscopic observations of SN 2019gsc.

Date	MJD	phase <sup>a</sup>	telescope <sup>b</sup>	range (nm)
2019-06-04	58638.47	1	NOT	350 ÷ 920
2019-06-11	58645.96	9	NOT	350 ÷ 920
2019-07-24	58688.90	52	GTC	350 ÷ 1000

<sup>a</sup> Phase is relative to the epoch of *g*-band maximum MJD = 58637.

<sup>b</sup> NOT = Nordic Optical Telescope, GTC = Gran Telescopio Canarias.

### 3 LIGHT CURVE ANALYSIS

The photometric evolution of SN 2019gsc in the better sampled *gri* bands are plotted in Fig. 2. Only the *r*-band light curve shows the rise to maximum. The luminosity decline is slower at longer wavelength (*i*-band) than at shorter ones (*g*-band). By using a low-order polynomial fit to the optical *g*- and *r*-band light curves around maximum (the first *i*-band point is at maximum) an estimate of the peak magnitude and epoch of maximum was obtained. Thanks to the inclusion of ZTF pre-maximum points or upper-limits, we find that SN 2019gsc reached an absolute magnitude at peak of  $M_g = -13.68 \pm 0.22$  mag ( $m_g = 19.98 \pm 0.20$  mag) on JD = 58637. The *r*-band peak occurred 4.2 d later at  $M_r = -14.25 \pm 0.25$  mag ( $m_r = 19.45 \pm 0.23$  mag). The uncer-

tainties in the absolute magnitudes are inferred propagating the errors of the fit to the peak apparent magnitudes and the errors in the adopted Galactic extinction and distance (cf. Section 2).

With the same polynomial fit we obtained a measure of the decline rate parameter  $\Delta m_{15}$ , the magnitude difference from the epoch of maximum brightness to 15 d later. SN 2019gsc has decline rates  $\Delta m_{15}(g) = 1.66 \pm 0.15$  mag and  $\Delta m_{15}(r) = 1.14 \pm 0.20$  mag. In the case of normal SNe Ia this parameter is known to correlate with luminosity (Phillips 1993), while in the case of SNe Iax the relation exhibits significant scatter (Foley et al. 2013). We find that SN 2019gsc does follow the general trend for SNe Iax, that is: fainter objects like SNe 2019gsc, 2008ha and 2010ae tend to exhibit narrower light curves, and their location on the  $\Delta m_{15}$  vs.  $M_r$  diagram (see for example Jha 2017, their Fig. 2) is in the bottom-right. Light curves parameters for SNe 2008ha, 2010ae and 2019gsc are reported in Table 4. At peak brightness, SN 2019gsc is  $\sim 0.3$  and  $0.9$  mag fainter than SN 2008ha in the *g*- and *r*-bands, respectively.

The extinction-corrected, *g-r* and *r-i* intrinsic colours of SN 2019gsc are plotted in Fig. 3. For comparison, the well-sampled, intrinsic colour curves of the type Iax SNe 2008ha (Stritzinger et al. 2014), 2005hk (Phillips et al. 2007; Stritzinger et al. 2015), 2010ae (Stritzinger et al. 2014), and 2014ck (Tomasella et al. 2016) are also included. The colour-curves are corrected for the Galactic and host

galaxy reddening, adopting extinction values of  $A_B = 0.03$  (SN 2019gsc), 1.23 (SN 2008ha), 0.45 (SN 2005hk), 2.54 (SN 2010ae), 2.05 (SN 2014ck) mag, and a standard  $R_B = 4.1$  reddening law (Cardelli, Clayton & Mathis 1989).

The best constraint on the rise time of SN 2019gsc comes from the early-phase  $g$ - and  $r$ -band magnitudes and upper-limits reported by ZTF in the *Lasair* broker. The pre-maximum portion of the  $r$ -band light curve (nine points) is fit with an *expanding fireball* model  $f_{model}(t) = \alpha(t - t_0)^n$ , with  $n = 2$  (Riess et al. 1999), similarly to what was done for SN 2014ck in Tomasella et al. (2016). From our best-fit to the early light curve of SN 2019gsc, we obtain  $t_0 = 58626_{-5}^{+3}$  MJD as the time of the first light. The reported uncertainty corresponds to the standard deviation of the  $t_0$  parameter when fitting a range of power laws, having  $1.8 \leq n \leq 2.2$ , to the pre-maximum  $r$ -band light curve, as the analysis of large SNe samples are found to be consistent with that spread of the  $n$  index (Piro & Nakar 2014). Consequently, SN 2019gsc has an  $r$ -band rise time  $t = 15_{-5}^{+3}$  d, and a  $g$ -band rise time  $\approx 11$  days ( $11_{-5}^{+3}$  d), applying the  $\sim 4$  days lag between  $g$  and  $r$  maximum.

We obtained an alternative estimate of the rise time of SN 2019gsc by stretching and then matching the  $r$ -band light curve to that of SN 2005hk, which has densely sampled multi-colour light curves and a very well constrained rise time to maximum (i.e.  $\approx 15$  days in  $B$  and  $\approx 22$  days in  $r$ -band; see Phillips et al. 2007). Thus, using a time stretching factor of about 0.7, the  $r$ -band rise time of SN 2019gsc is estimated to be  $\approx 15$  days, consistent to the value inferred by polynomial fit.

### 3.1 Bolometric light curve and energetics

Using the *griz*-band photometry of SN 2019gsc, we construct a pseudo-bolometric light curve. The photometry obtained at each epoch was converted to flux at the effective wavelength of its corresponding passband. If photometry was not available in a given filter on a particular night, a magnitude was estimated through interpolation between adjacent epochs, or if necessary, by extrapolation assuming a constant colour from the closest available epochs. The fluxes were then corrected for reddening, yielding the spectral energy distribution (SED) at each epoch. These SEDs were integrated using a trapezoidal integration algorithm, assuming zero flux at the integration boundaries. Finally, the flux at each epoch was converted to luminosities using our adopted distance to the host galaxy (see Table 1).

Unfortunately, no ultraviolet (UV) nor near-IR (NIR) observations of SN 2019gsc were taken, and only a few  $u$ -band upper-limits were collected during our follow-up campaign. The  $u$  and NIR-band contributions to the SEDs were therefore inferred from the ratio in flux between the OIR and optical-band bolometric light curves constructed for SNe 2002cx, 2008ha and 2010ae, in analogy to the procedure followed in Tomasella et al. (2016, cf. their Section 6.3). The  $u$ - and NIR-band contributions is estimated as 35% at maximum light, decreases to about 8% ten days after, and drops to zero soon after. By summing this contribution to the initial *griz*-band pseudo-bolometric light curve of

SN 2019gsc, we obtaining the OIR<sup>9</sup> bolometric light curve plotted in Fig. 4. For comparison, the OIR bolometric light curves of SNe 2008ha, 2010ae, and 2002cx are also plotted in Fig. 4. The OIR light curves of the comparison objects are computed following the same prescription adopted for SN 2019gsc, making use of the photometry, reddening values, and distances found in the literature (i.e.,  $E(B - V)_{tot} = 0.3$  mag,  $\mu = 31.55$  mag for SN 2008ha from Stritzinger et al. 2014;  $E(B - V)_{tot} = 0.62$  mag,  $\mu = 30.58$  mag for SN 2010ae from Stritzinger et al. 2014;  $E(B - V)_{tot} = 0.034$  mag,  $\mu = 35.09$  mag for SN 2002cx from Li et al. 2003;  $H_0 \equiv 73$  km s<sup>-1</sup> Mpc<sup>-1</sup>).

The OIR peak luminosity of SN 2019gsc is  $L_{max} = 8.9 \pm 2.5 \times 10^{40}$  erg s<sup>-1</sup>. By definition, the OIR does not include any UV contribution. We remark that SN 2005hk and SN 2012Z were detected in the UV at very early phases, but they both faded below the detection limit well before the epoch of optical maximum (Phillips et al. 2007; Brown et al. 2009; Stritzinger et al. 2015). This implies that, in both objects, the flux in the UV drops below 10% of the total flux before maximum. In general, SNe Ia are bluer than normal SNe Ia in the UV before maximum light, but quickly redden (by  $\sim 1.5 - 2$  mag in *Swift uuv1-b*). Hence,  $\sim 10$  days post maximum, they are already redder than normal SNe Ia (Jha 2017). Thus, if we would consider a maximum of 10% for the contribution of the UV flux to the peak luminosity of SN 2019gsc, we obtain  $L_{max,19gsc} \approx 9.8 \times 10^{40}$  erg s<sup>-1</sup>. In any case, SN 2019gsc remains an extremely low-luminosity event, very similar to SN 2008ha for which a peak luminosity  $L_{max,08ha} \approx 9.5 \times 10^{40}$  erg s<sup>-1</sup> was reported (Valenti et al. 2009; Foley et al. 2009; Stritzinger et al. 2014), but without considering any UV contribution.

With the assumption that the light curve of SN 2019gsc is powered by <sup>56</sup>Ni decay, the amount of <sup>56</sup>Ni synthesized during the explosion is estimated using Arnett's rule (Arnett 1982). See Stritzinger & Leibundgut (2005), their Section 4, for an analytical expression that links <sup>56</sup>Ni mass to the peak bolometric luminosity. Adopting the  $B$  band  $\approx 11$  days rise time and a peak luminosity of  $9.8 \times 10^{40}$  erg s<sup>-1</sup>, which includes the UV contribution, and with the assumptions described in Arnett (1982), we obtain the crude estimate of  $M_{Ni} \approx 0.003 \pm 0.001 M_{\odot}$ . Here the quoted error is largely due to the uncertainties in the rise time and in the adopted distance, which contribute by  $\sim 20$  and  $\sim 15$  per cent to the total error budget, respectively.

Compared to normal SNe Ia and to the prototype SN 2002cx, the low expansion velocity of SN 2019gsc ejecta ( $v_{ph} \approx 3.5 \times 10^3$  km s<sup>-1</sup>, cf. Section 4 and Fig. 8) suggests it also has much lower ejecta mass ( $M_{ej}$ ) and kinetic energy ( $E_k$ ). Quantitatively, the explosion parameters providing a good match to the bolometric light curve of SN 2019gsc are  $M_{ej} \approx 0.13 M_{\odot}$  and  $E_k \approx 12 \times 10^{48}$  erg, using Arnett's equations Arnett 1982 as done in Valenti et al. 2009 and Foley et al. 2009 for SN 2008ha. The value of these explosion parameters are similar to values inferred for both SN 2008ha and SN 2010ae.

<sup>9</sup> OIR stands for Optical-to-InfraRed and extends from the ground-based  $u$  band to the  $K$  band

**Table 4.** Light curves parameters for SN 2019gsc (this work), SN 2008ha, and SN 2010ae (Stritzinger et al. 2014). The absolute magnitudes range for SN 2010ae depends on the adopted extinction.

Filter	$m_{peak}$ (mag)	$M_{peak}$ (mag)	$\Delta m_{15}$ (mag)
<b>SN 2019gsc</b>			
<i>g</i>	19.98 (0.20)	-13.68 (0.22)	1.66 (0.15)
<i>r</i>	19.45 (0.23)	-14.25 (0.25)	1.14 (0.20)
<b>SN 2010ae</b>			
<i>g</i>	17.49 (0.02)	-13.54/-15.33 (0.54)	1.51 (0.05)
<i>r</i>	16.92 (0.23)	-13.99/-15.29 (0.54)	1.01 (0.03)
<b>SN 2008ha</b>			
<i>g</i>	17.87 (0.02)	-14.01 (0.14)	1.80 (0.03)
<i>r</i>	17.67 (0.01)	-15.15 (0.14)	1.11 (0.04)

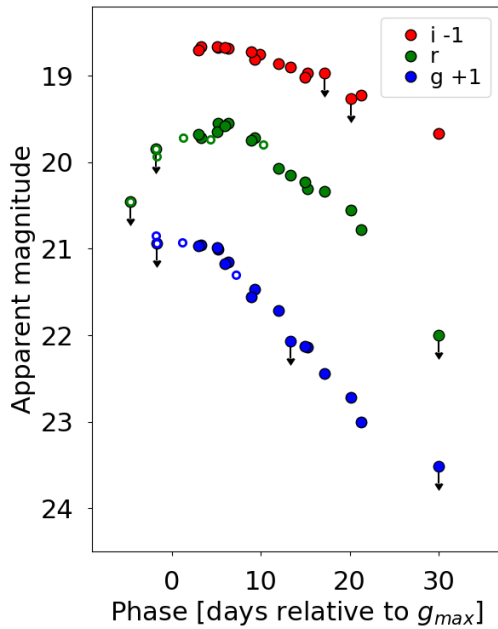


**Figure 2.** Optical *gri*-bands light curves of SN 2019gsc in the AB system. For clarity, the light curves have been shifted vertically as indicated in the legend. The open circles correspond to photometric points taken from the ZTF archive (cf. Table 2). Epochs with arrows are upper-limits.

#### 4 SPECTROSCOPIC ANALYSIS

Our spectroscopic time series of SN 2019gsc consists of three optical spectra obtained at maximum light, nine days and about fifty days post maximum. The last spectrum was taken when the object had faded to a magnitude of  $m_r \approx 22$  mag. The spectroscopic sequence is shown in Fig. 5.

The first spectrum taken at maximum light exhibits a blue continuum (the blackbody temperature is  $T_{bb} \approx 9 \times 10^3$  K, cf. Fig. 8) superposed with a rich structure, along with several low-velocity P-Cygni features associated with both intermediate-mass elements (IMEs) and Fe-group elements. By comparison with normal SNe Ia and using SYNOW (Branch et al. 2004) synthesis code for fitting our spectra to

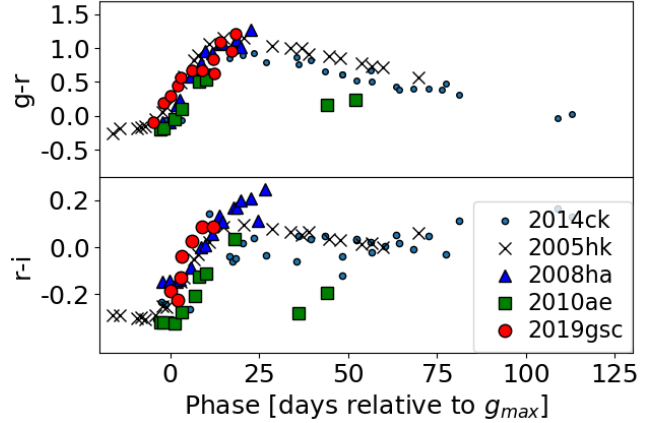


**Figure 3.** The  $g-r$  and  $r-i$  (AB mag) extinction-corrected colour curves of SN 2019gsc compared with those of SNe 2008ha, 2010ae, and 2005hk (Stritzinger et al. 2014, 2015), and SN 2014ck (Tomasella et al. 2016).

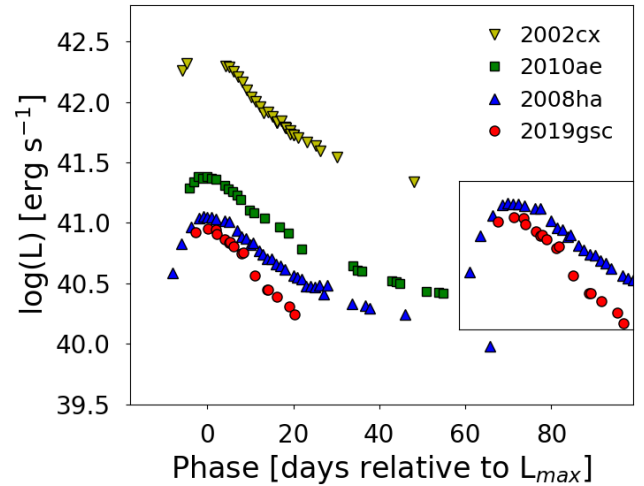


**Figure 4.** Pseudo-bolometric light curve of SN 2019gsc constructed by integrating over the *griz*-band flux points. The contribution to the total flux from the unavailable *u* and NIR bands was estimated (and added) from the ratio in flux between the OIR (Optical-to-Infrared) and the optical pseudo-bolometric light curves of SNe 2002cx, 2010ae, 2008ha, which are also plotted for comparison (see text for details). The inset shows a zoomed view comparing the early bolometric light curves of SNe 2008ha and 2019gsc.

profile of various ions, we identify: a relatively weak and narrow Si II  $\lambda 6355$  feature, along with absorptions attributed to Ca II H&K and Ca II NIR triplet; Si II  $\lambda \lambda 5454, 5640$ ; Na I D; O I  $\lambda 7774$  line (which is visible from day +1 to +52); high-ionization lines of Fe II, Co II and Fe III which seems to produce most of the observed features blueward of  $\sim 5000$  Å; and, possibly, C II  $\lambda \lambda 6580, 7234$ . There is some indication that early spectra of type Ia SNe contain C II and, sometimes, also C III (i.e. Chornock, et al. 2006; Foley et al. 2013; Tomasella et al. 2016). Actually, we obtain a reasonable fit

to absorption features at  $\sim 6580$  and  $7230 \text{ \AA}$  adding C II ion in SYNOW spectral model (rather than other ions, i.e. Fe II), as it is shown in the inset of Fig. 5. If this identification is correct, the detection of C II in the ejecta of SN 2019gsc might be related to unburnt material of the progenitor system, giving indication on its nature (C/O WD *vs* O/Ne/Mg WD; see Nomoto, Kamiya & Nakasato 2013), or on the mechanism by which the explosive flame propagates throughout the WD (Folatelli et al. 2012).

As for the other members of the SN Iax class, we find no evidence for hydrogen. Conversely, Magee et al. (2019) investigated the prospect to detect helium features in SNe Iax spectra following the notion that their progenitor are C/O WDs accreting material from helium star companions (Foley et al. 2013; McCully et al. 2014). They conclude that the best chance for detecting He I features is either at NIR wavelength during early phases, or in post-maximum spectra of the fainter members of the class. Being among the faintest SN Iax yet observed, SN 2019gsc offers an excellent opportunity to search for signatures of helium, although unfortunately no NIR spectrum was taken close to maximum when the strongest He I feature, at  $\lambda 10830$  is expected to be most prevalent.

We used the SYNOW spectral synthesis code to model the optical spectra taken at one and nine days post maximum, but were unable to find conclusive evidence for the presence of helium lines, such as He I  $\lambda 5876$ ,  $\lambda 6678$  or  $\lambda 7065$ . We further investigate the possible signature of helium in SN 2019gsc comparing the +9 d spectrum with the synthetic N5def-hybrid models calculated by Magee et al. (2019) specifically for the faintest members of the SN Iax class. Their N5def-hybrid models are based on TARDIS radiative transfer code (Kerzendorf & Sim 2014) and on the multi-dimensional explosion simulations of Fink et al. (2014) and Kromer et al. (2015). In this explosion scenario, the C-O core is surrounded by an O-Ne mantle, which stops the propagation of the deflagration front and therefore only a small amount of  $^{56}\text{Ni}$  is produced, of the order of  $3 \times 10^{-3} M_{\odot}$ , as actually obtained for SNe 2008ha, 2010ae and 2019gsc. In Fig. 6 we show the zoom-ins of the regions surrounding He I  $\lambda 5876$ ,  $\lambda 6678$  and  $\lambda 7065$  of SN 2019gsc spectrum at phase +9 d and the comparison with Magee et al. (2019) N5def-hybrid model at similar phase. From the similarities of the observed and model features, we find marginal evidence of helium in SN 2019gsc, despite the low signal-to-noise ratio of our spectrum. We notice that a best match is with the N5def-hybrid model (red line in Fig. 6) which has a higher helium abundance (36%), corresponding to a few  $10^{-2} M_{\odot}$ . He I lines are fitted by a P-Cygni profile.

We note here that the spectroscopic modelling, based on synthetic code SYNAPPS (Thomas, Nugent & Meza 2011), of 44 SNe Iax by Jacobson-Galán et al. (2019) confirms the detection of He I lines in the early-time optical spectra of SNe 2004cs and 2007J, as previously reported by Filippenko et al. (2007); Foley et al. (2016); Magee et al. (2019). Jacobson-Galán et al. (2019) highlight that these He I features are better fit by a pure-emission Gaussian rather than a P-Cygni profile, suggesting a circumstellar origin of helium. Actually, the presence of a dense circumstellar medium (CSM) was proposed for explaining the strong mid-IR excess observed for the type Iax SN 2014dt, which would be consistent with either newly formed dust, or pre-explosion mass loss (Fox et

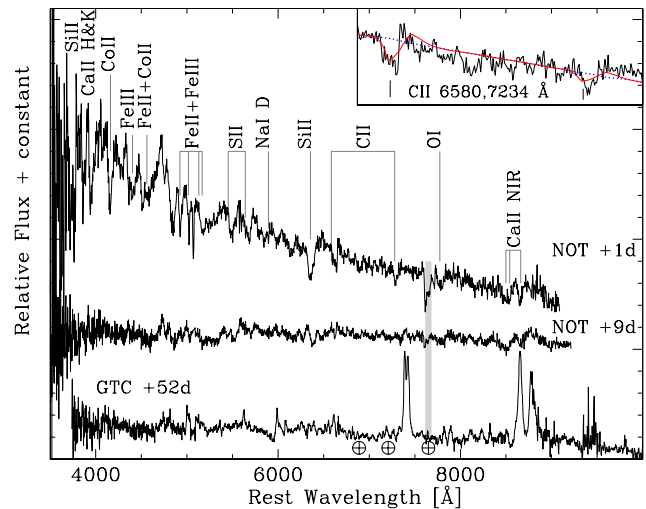


**Figure 5.** Spectroscopic sequence of SN 2019gsc, along with line identification of prominent features. The inset on the top shows the region of the +1d spectrum (black) centered on C II  $\lambda 6580$ ,  $7234$ , with overplotted the SYNOW synthetic spectra of the C II (solid red line) and Fe II ions (dotted blue).

al. 2016). On the other hand, deep radio observations of the nearby type Iax SN 2012Z by Lundqvist et al. (2020) and Chomiuk et al. (2016, they also report data on SN 2008ha, but not so deep to be significant), and SN 2019muJ by Perez-Torres et al. (2019) find no evidence of radio emission: the debate of CSM in type Iax SNe is still open.

In Fig. 7 the spectra of SN 2019gsc are compared with those of the fast-and-faint type Iax SNe 2008ha and 2010ae at similar phases. Notably, all spectra are very similar at maximum light and one week later, while about fifty days after maximum, forbidden calcium emission lines are strong in SNe 2019gsc and 2008ha, while in SN 2010ae they are relatively weak and emerge only during later epochs (see Section 4.1).

#### 4.0.1 Expansion velocities of the ejecta

The low expansion velocity of the ejected material is a hallmark of SNe Iax and is indicative of low-explosion kinetic energy in comparison to normal SNe Ia, as previously noted in Sect. 3.1. The ejecta velocity of SN 2019gsc is estimated from the location of the absorption minimum of Si II  $\lambda 6355$ , which suffers negligible line blending relative to other features in the spectrum. We measure a Si II expansion velocity of  $v_{ph} \approx 3,500 \text{ km s}^{-1}$  at the time of g-band maximum and this decreases to  $v_{ph} \approx 2,400 \text{ km s}^{-1}$  nine days later. In Fig. 8 (bottom panel) the expansion velocity evolution of the three faintest SN Iax, SNe 2008ha, 2010ae, and 2019gsc, is compared with the prototypical type Iax SN 2002cx. We conclude that the expansion velocities of SN 2019gsc are similar to those of SN 2008ha, and about  $\sim 20\%$  and  $\sim 40\%$  slower than SN 2010ae and SN 2002cx, respectively.

Taking the Si II  $\lambda 6355$  absorption line as an indicator of the photospheric velocity, the ratio between the Doppler velocity of the putative C II  $\lambda 6580$  and Si II  $\lambda 6355$  at maximum is  $\sim 0.5$  (cf. Fig. 8), which is similar to that observed in SN 2008ha (Parrent et al. 2011). This ratio is generally

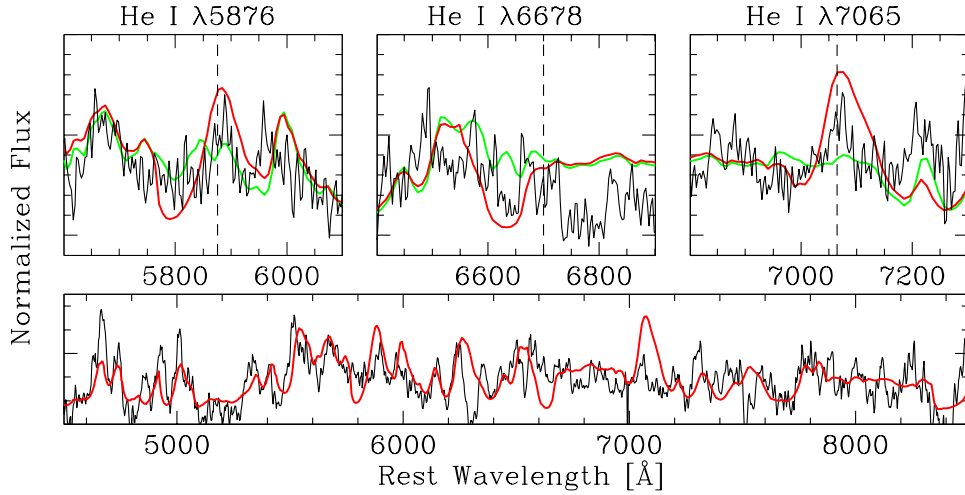


**Figure 6.** Comparison of the +9 d spectrum of SN 2019gsc with the N5def-hybrid models by Magee et al. (2019) with 0.22% (green line; top panels) and 36% (red line; top and bottom panels) helium abundances. On top, from left to the right the panels show the wavelength regions of He I  $\lambda$ 5876,  $\lambda$ 6678 and  $\lambda$ 7065, respectively.

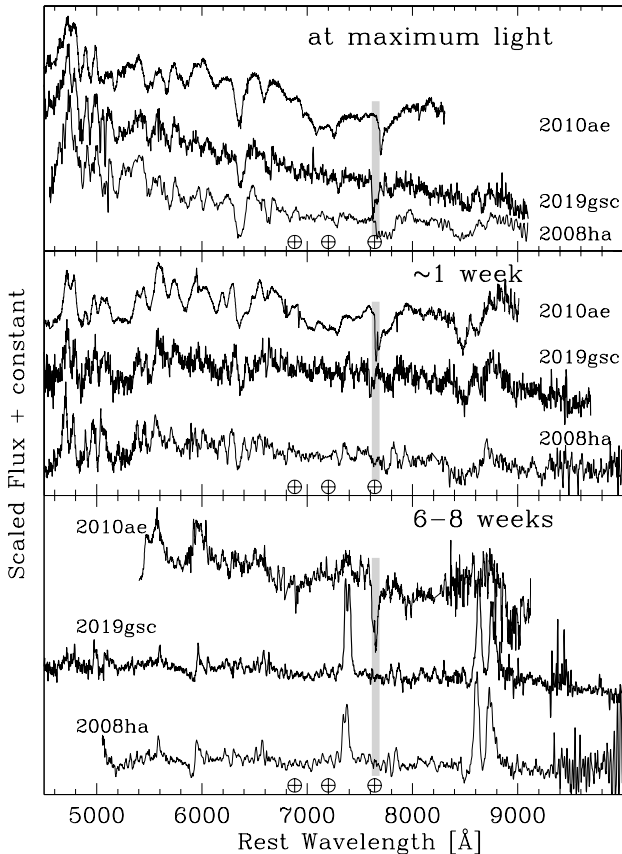


**Figure 7.** Sequences of spectra of the faint type Iax SNe 2019gsc, 2010ae, and 2008ha at similar phases, extending from around maximum light, to one week, and finally out to 6–8 weeks post maximum. The spectra of SN 2008ha are from Valenti et al. (2009) and those of SN 2010ae from Stritzinger et al. (2014).

slightly above unity in normal SNe Ia (Folatelli et al. 2012);  $\sim 0.89$  and  $\sim 0.95$  in SN 2012Z and SN 2014ck, respectively (Stritzinger et al. 2015; Tomasella et al. 2016). The fact that the C II Doppler velocity is significantly lower than the photospheric velocity may indicate ejecta asymmetries as suggested by Foley et al. (2016) for SN 2008ha, or alternatively the line is not associated with C II.

Also plotted in Fig. 8 (top panel) are the estimates of the photospheric temperature of SN 2019gsc as derived from a blackbody (BB) function fit to the spectral continuum. Only the first two epochs were considered, as at +52 d the presence of emission lines and line blanketing drive a flux deficit at shorter wavelengths. Spectra were corrected for redshift and extinction before the fit. Errors are estimated from the dispersion of measurements obtained with different choices for the spectral fitting regions. The photospheric temperature of SN 2019gsc at maximum is around 8,000 K to 9,000 K, rapidly decreasing below 6,000 K one week later, similar to the BB temperature evolution of SNe 2008ha and 2010ae.

#### 4.1 The Gran Telescopio Canarias late-time spectrum

We observed SN 2019gsc with the Gran Telescopio Canarias (GTC) equipped with OSIRIS and using the R1000B+R1000R grisms (DDT-GTC2019-129, PI N. Elias-Rosa). This setup provided wavelength coverage from 363.0 nm to 1000 nm. The observations were carried out on 2019 July 24, when the SN was +52 d post-maximum and its brightness around  $m_r \sim 22$  mag, with a total integration time of 2 hours.

The high-quality GTC spectrum of SN 2019gsc exhibits the late-time spectral characteristic of the SN Iax class, consisting of a weak continuum superposed with both permitted and forbidden emission lines (Foley et al. 2016). The best match is with the faint SN Iax SN 2008ha at similar phase (cf. Fig. 9, top-left panel).

As shown in Fig. 9, the late-time spectrum of

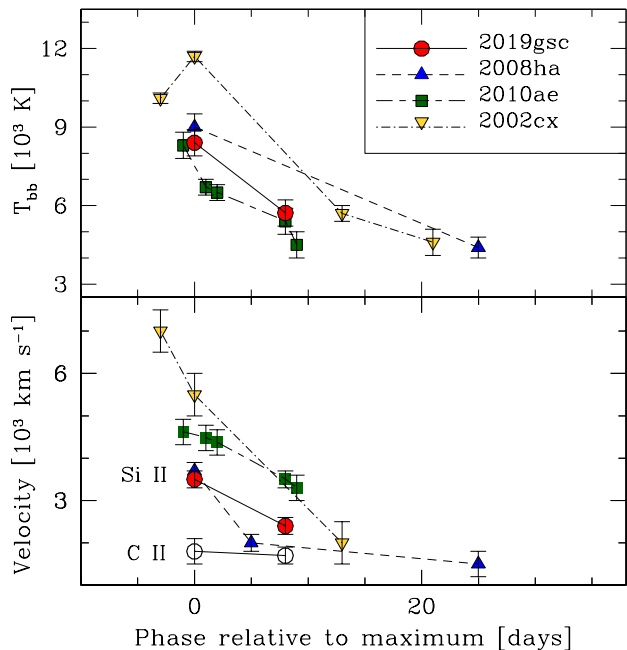


**Figure 8.** Top-panel: comparison of the time evolution of  $T_{bb}$  for SN 2019gsc with SNe 2008ha, 2010ae and 2002cx. Bottom-panel: expansion velocity evolution of the ejecta of SN 2019gsc, estimated measuring the location of the absorption minimum of Si II  $\lambda 6355$  (filled red circles) and C II  $\lambda 6580$  (open circles). Si II  $\lambda 6355$  velocity for SN 2008ha (filled blue triangles), SN 2010ae (filled green squares) and SN 2002cx (filled yellow triangles) are also reported.

SN 2019gsc is also similar to that of the brighter type Iax SN 2014ck (peak  $V$  mag  $-17.29$ , Tomasella et al. 2016) taken at a phase of  $+166.3$  d, thus highlighting the very rapid spectroscopic evolution of the fainter members of the SN Iax class.

Following Li et al. (2003); Jha et al. (2006); Sahu et al. (2008), we identify narrow, permitted Fe II features and a number of forbidden lines associated to iron, cobalt and calcium (see Fig. 9). The strongest features are attributed to calcium, including both the Ca II NIR triplet and the forbidden [Ca II]  $\lambda\lambda 7292, 7324$  doublet. Both permitted and forbidden calcium lines are significantly more prominent in SN 2019gsc than SN 2002cx taken at a similar phase, and are comparable to those of SN 2008ha. As for SNe 2002cx (Jha et al. 2006) and 2005hk (Sahu et al. 2008), several weak O I lines are tentatively recognized in SN 2019gsc until late phase (see Fig. 9, bottom-panel), suggesting that the elements in the ejecta are homogeneously mixed. In contrast, forbidden oxygen features [O I]  $\lambda\lambda 6300, 6364$  are not detected in this late-time spectrum of SN 2019gsc (so far [O I] has never been observed in SNe Iax, cf. Jha et al. 2006; McCully et al. 2014; Foley et al. 2016). It was suggested that [Ca II]  $\lambda\lambda 7292, 7324$  can limit the strength of [O I]  $\lambda\lambda 6300, 6364$  emission from a region in which both these ions co-exist Dessart & Hillier (2015, and references therein). In passing, we note that normal stripped-envelope, core-collapse SNe exhibit strong [O I] emission at late times. The absence of forbidden oxygen in the late-time spectra of SNe Iax weak-

ens the link with core-collapse SNe which have been also considered a possible explanation for SNe Iax (Valenti et al. 2009; Moriya et al. 2010).

We fit Gaussian profiles to the [Ca II], [Fe II] and Ca II NIR features, which are characterised by a narrow component, having a full-width-half-maximum (FWHM) velocity of 1400, 1100 and 1500 km s<sup>-1</sup>, respectively. These nebular lines have slightly different velocity shifts relative to the rest frame, ranging from about  $+130$  km s<sup>-1</sup> for [Fe II]  $\lambda\lambda 7155, 7453$ , and  $-280$  km s<sup>-1</sup> for [Ca II]  $\lambda\lambda 7291, 7324$ . These shifts in opposite directions of [Fe II] and [Ca II] features suggest a complex structure of the SN 2019gsc ejecta. Similar velocity shifts were observed in many other SN Iax late-time spectra (Foley et al. 2016).

To summarise, we find that the  $+52$  d spectrum of SN 2019gsc is similar to those of other SNe Iax at least half a year post maximum. This is an exceptionally fast spectral evolution, similar to SN 2008ha, but not to SN 2010ae (Stritzinger et al. 2014), which does not exhibit forbidden Ca II emission at the same phase (cf. Fig. 9).

## 5 ENVIRONMENTS OF FAINT TYPE IAX SNE

SNe Iax are usually found in star-forming, late-type host galaxies. Lyman et al. (2018) have recently performed spectroscopic environmental measurements of the host galaxies and the explosion sites for about twenty SNe Iax (see their Table 1). They find that the metallicity distribution of the SN Iax explosion site is similar to that of core-collapse SNe, and metal poor in comparison to normal SNe Ia as well as spectroscopically classified 1999T-like objects. Moreover, fainter members of the SN Iax class are found to be located in very metal poor environments. However, their sample contains a small number of very faint objects and consequently the statistics are limited. New SNe Iax are crucial to gain further information on this topic, and, in this respect, the extremely-faint SN 2019gsc is particular interesting.

In order to derive the metallicity for the host galaxy of SN 2019gsc and for its explosion site, we use spectra downloaded from SDSS DR12 as well as our own GTC spectrum (cf. Sect. 4.1), and the calibration of Pettini & Pagel (2004) or Marino et al. (2013). These authors calibrate the oxygen abundances of extra-galactic H II regions for which the oxygen abundance was determined with the direct  $T_e$ -based method against the  $N2$  and  $O3N2$  indices:  $N2 \equiv \log_{10}([\text{N II}]\lambda 6583/\text{H}\alpha)$  and  $O3N2 \equiv \log_{10}([\text{O III}]\lambda 5007/\text{H}\beta)/([\text{N II}]\lambda 6583/\text{H}\alpha)$ . The  $N2$  and  $O3N2$  indices have the advantage over other types of calibrations in the literature due to the small wavelength separation between the lines, and hence are less sensitive to the extinction and to issues related to flux calibration.

When using the archive spectra of SBS 1436+529A, the emission line flux measurement (as described in Lyman et al. 2018, their Section 3.3), provides the indices  $N2 = -1.43 \pm 0.03$  and  $N2O3 = 2.04 \pm 0.04$ . Thus, we estimate the SN 2019gsc host-galaxy oxygen abundance to be: (i)  $12 + \log_{10}(\text{O}/\text{H}) = 8.08 \pm 0.01$  dex, using the calibration for  $O3N2$  of Pettini & Pagel (2004); or (ii)  $12 + \log_{10}(\text{O}/\text{H}) = 8.10 \pm 0.01$  dex, using the calibration for  $O3N2$  of Marino et al. (2013). The reported errors on metallicity are formal errors. Added the

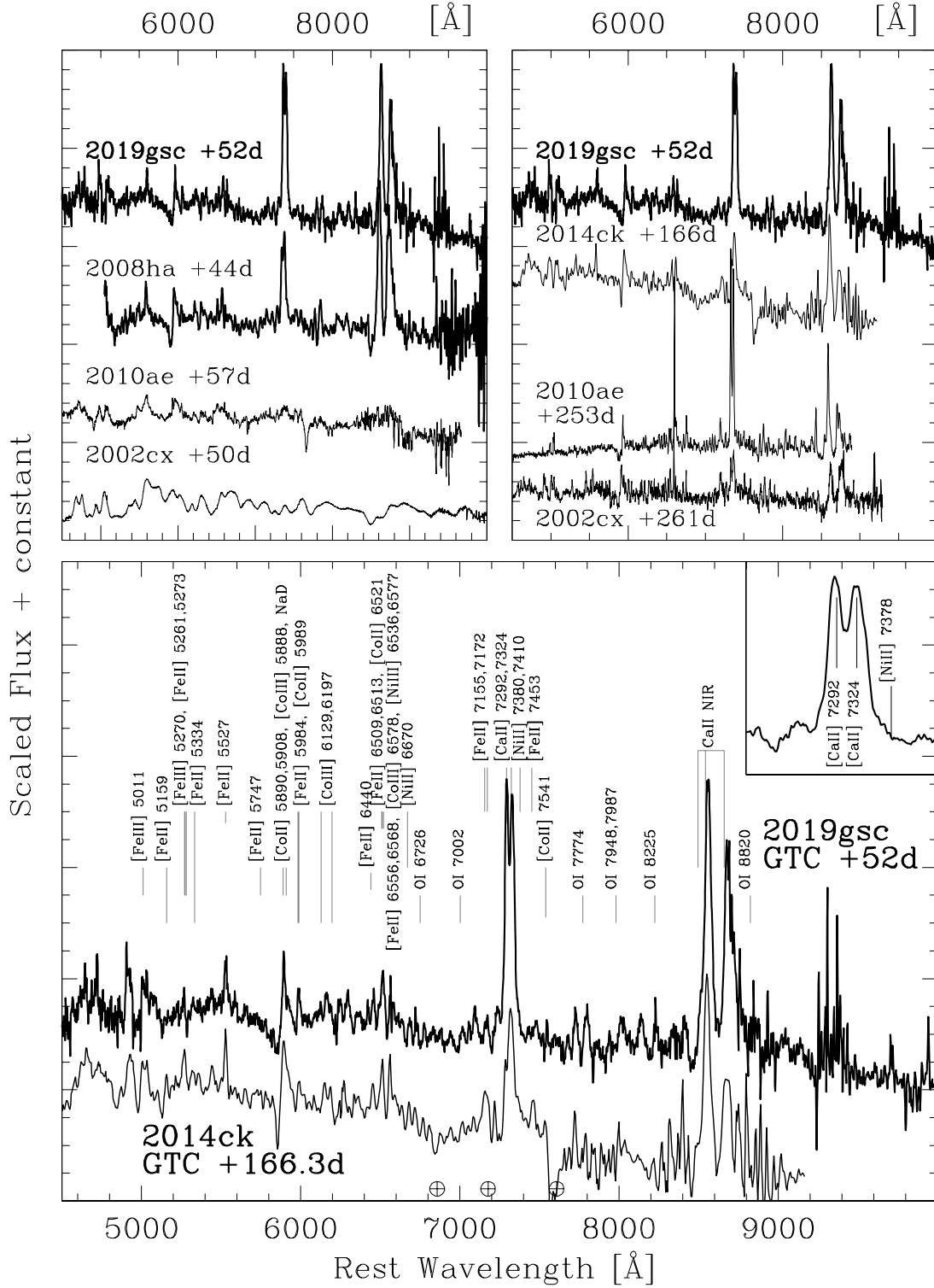


**Figure 9.** Top-left panel: comparison of the +52 d GTC spectrum of SN 2019gsc with similar phase spectra of SN 2008ha (Valenti et al. 2009), SN 2010ae (Stritzinger et al. 2014), and the prototype of the class SN 2002cx (Li et al. 2003). Top-right panel: the same spectrum of SN 2019gsc is compared with the spectra of the brighter type Ia SN 2014ck (Tomasella et al. 2016) and SN 2002cx, and with the faint SN 2010ae, taken at phases > 5 months. Bottom-panel: zoomed-view of the GTC late-spectrum of SN 2019gsc, with line identification based on Li et al. (2003), Jha et al. (2006) and Sahu et al. (2008). The inset shows the region centered on [Ca II]  $\lambda$ 7292, 7324 doublet. The position of (weak/absent) [Ni II]  $\lambda$  7378 is marked.

**Table 5.** Estimates for SN 2019gsc host-galaxy and explosion-site metallicity, using the calibration for  $O3N2$  by Marino et al. (2013).

$z$ host galaxy nucleus	$8.10 \pm 0.18$ dex
$z$ SN site 1	$8.23 \pm 0.18$ dex
$z$ SN site 2	$8.17 \pm 0.18$ dex

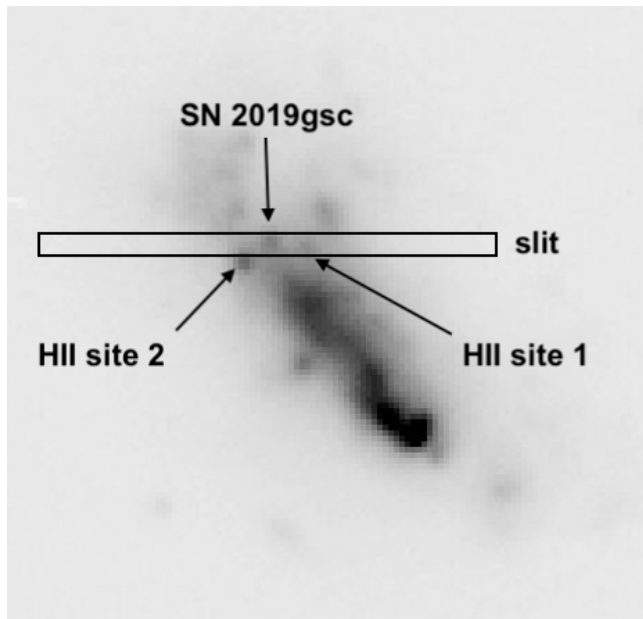


**Figure 10.** Slit position during the acquisition of the GTC spectrum of SN 2019gsc. Bright H II regions on the right (site 1) and on the left (site 2) of the SN were also captured.

formal errors in quadrature with systematic errors related to determining the gas-phase metallicity, i.e.,  $\approx 0.16 - 0.18$  dex (Marino et al. 2013), we obtain  $z_{nucleus,19gsc} = 8.10 \pm 0.18$  dex. This value is sub-solar (using  $12 + \log_{10}(O/H) = 8.69$  dex as the solar abundances, see Asplund et al. 2009).

As our GTC long-exposure (2 hours), long-slit spectrum includes also the bright H II regions both on the left and on the right of the position of the SN location (see Fig. 10), we extracted a 1-D spectrum for each H II region. Thus, we derive the metallicity for the H II regions close to the SN 2019gsc explosion site using the individual line fluxes, in the same manner as done with the host-galaxy spectrum. We report the results in Tab. 5 and note that they too suggest a sub-solar metallicity. All three of our metallicity estimates are in agreement within the errors.

These measurements place the SN 2019gsc on the metal-poor tail of the metallicity distribution for the SNe Iax collection by Lyman et al. (2018, cf. their Table 4). Actually, the host galaxy of SN 2019gsc has the lowest inferred metallicity in comparison to values obtained at both the SN explosion sites and host nuclei of the Lyman et al. (2018) sample, and is very similar to the metallicity deduced from the explosion site of SN 2008ha, i.e.,  $z_{site,08ha} = 8.22 \pm 0.18$  dex.

As a test case, we also download the host spectrum of SN 2010ae, ESO 162-017; from 6DF Galaxy Survey, via

NED)<sup>10</sup>, and estimated an oxygen abundance of  $z_{host,10ae} = 8.32 \pm 0.18$  dex using  $O3N2$  index and the Marino et al. (2013) calibration. This is in full agreement with the value of  $8.34 \pm 0.14$  dex measured by Stritzinger et al. 2014 and  $8.31 \pm 0.18$  dex by Lyman et al. 2018.

## 6 CONCLUSIONS

The observations presented in this paper provide a view on an extreme member of the class of faint-and-fast evolving SNe Iax that includes SN 2008ha, SN 2010ae, and even SN 2009J (Foley et al. 2013). SN 2019gsc is characterized by an extremely low luminosity, reaching an absolute peak  $g$ -band magnitude of only  $M_g = -13.68 \pm 0.22$  mag (it is  $M_g = -14.01 \pm 0.14$  mag for SN 2008ha), displays a fast evolving light curve ( $\Delta m_{15}(g) = 1.66 \pm 0.15$ ), and a  $g$ -band rise time of  $\approx 11^{+3}_{-5}$  d. It also exhibits low expansion velocity of the ejecta, about  $\sim 3,000$  km s<sup>-1</sup> at maximum, and consequently low kinetic energy, similar to SN 2008ha. Also similarly to SNe 2008ha and 2010ae, the peak of the pseudo-bolometric light curves indicates that all three faint-and-fast SN Iax produced around a few  $\times 10^{-3} M_{\odot}$  of <sup>56</sup>Ni.

In many ways, SN 2019gsc is a clone of the exceptional and still enigmatic SN 2008ha (Foley et al. 2016). Thus, it enters in the debate concerning the nature and origins of these events: core-collapse or thermonuclear explosions? (Valenti et al. 2009; Foley et al. 2009; Moriya et al. 2010; Foley et al. 2016). Recently, there have been some exploration of the explosion scenarios that can produce rapidly-evolving faint transients, even fainter than the faintest SNe Iax. These include the outcomes of stripped-envelope electron-capture SNe (ECSNe, Moriya & Eldridge 2016), as well as a double-degenerate scenario consisting of the merger of a carbon-oxygen and a oxygen-neon WD (Kashyap et al. 2018). However, to date no spectral modelling for ECSNe (Moriya & Eldridge 2016) is available and the published synthetic light curve do not cover a range in peak luminosity. Moreover, while the light curve properties and ejecta velocities of the faintest SNe Iax may appear to be somewhat consistent with stripped-envelope ECSNe model, we stress that the post maximum NIR spectroscopic sequence, obtained by Stritzinger et al. (2014) for SN 2010ae as well as for the brighter SN 2014ck in Tomasella et al. 2016, indicates the presence of Co II and hence provides a stronger link to thermonuclear explosions. Despite the lack of NIR spectra for SN 2019gsc, as well as for SN 2008ha, the striking spectral similarities in the visual-wavelength range with both the faint SNe 2008ha, 2010ae, and the brighter SNe 2002cx and 2014ck (when comparing spectra at different epochs, cf. Fig. 9), suggest a similar explosion mechanism for the broad class of SNe Iax.

We stress that the spectroscopic evolution of SN 2019gsc is unusually rapid, as strong forbidden iron, nickel, calcium emission lines have clearly emerged in the spectrum taken on +52 d. Equally strong at this epoch are the permitted Ca II NIR triplet features. Our late-time spectrum perfectly matches the similar-phase (+44 d) spectrum of SN 2008ha, while SN 2010ae, and other brighter SNe Iax, exhibit calcium

<sup>10</sup> <http://www.6dfgs.net/>

lines at a later phase. At any rate, the fainter SNe 2019gsc and 2008ha are spectroscopically similar, if compared at different phases, either to the equally faint SN 2010ae and to brighter objects such as SNe 2002cx and 2014ck, plotted in Fig. 9. More explicitly, the spectra of SNe 2008ha and 2019gsc  $\gtrsim 1$  month post maximum share the general shape as other SNe Iax at phases  $\gtrsim 5 - 6$  months post maximum.

However, as highlighted by Foley et al. (2016), there is also significant diversity in the late-time spectra of SN Iax class, especially in the strength, width and line shifts of forbidden emissions, such as [Ca II]  $\lambda\lambda 7291, 7324$ , [Fe II]  $\lambda 7155$ , and [Ni II]  $\lambda 7378$ . Foley et al. (2016) proposed a two-component model where the photosphere, P-Cygni and narrow forbidden lines are produced by the wind, while the broad forbidden lines comes from the SN ejecta. In this perspective, SN 2019gsc belongs to low velocity, weak (or absent) [Ni II], strong and narrow [Ca II] group (cf. Fig. 9), as well as SN 2008ha, but also the bright prototype Iax SN 2002cx (Foley et al. 2016, cf. their Section 3). The deflagration of a  $M_{Ch}$  hybrid carbon-oxygen-neon WD, leaving behind a bound remnant (Kromer et al. 2015) might produce faint transient (i.e., having peak absolute  $B$  magnitudes in the range  $-13.2$  to  $-14.4$  mag) with observational characteristics similar to both SNe 2008ha and 2019gsc, though there are shortcomings, for example the spectro-photometric evolution of the model is too fast. A possible alternative is the merger of a oxygen-neon and carbon-oxygen WD (double-degenerate channel) that yields a failed detonation and produces a very faint, rapidly fading transient (actually fainter than SNe 2008, 2010ae and 2019gsc) with a small  $^{56}\text{Ni}$  and ejecta mass (see Kashyap et al. 2018, for details).

We note that recently Vennes et al. (2017) and Raddi et al. (2019) have discovered a handful of high proper motion, low-mass Galactic WDs traveling at a velocity greater than the Milky Way escape velocity and whose peculiar atmospheres are dominated by IMEs. These authors argue that these inflated and IME contaminated WDs are the partially burnt remnants of SNe Iax, which have survived and were ejected from a binary SN progenitor system with a high kick velocity. The possible weak signature of He I lines in the post-maximum spectrum of SN 2019gsc (cf. Fig. 6) may indicate a WD-He star binary progenitor system, consistent with the idea that the faintest SN Iax are associated with the partial disruption of their progenitor stars, while the brightest objects may be linked to the full disruption of a Chandrasekhar mass WD (e.g., Sahu et al. 2008; Stritzinger et al. 2015). Further study of exceptionally faint SNe Iax is critical to constrain their progenitors and explosion mechanisms.

## ACKNOWLEDGEMENTS

Special thanks to the GTC Director and Support Staff for executing observations under director discretionary program DDT-GTC2019-129 (P.I. N. Elias-Rosa). M.S. is supported by a generous grant (13261) from the VILLUM FONDEN and a project grant from the Independent Research Fund Denmark (IRFD; 8021-00170B). K.M. acknowledges support from H2020 ERC grant no. 758638. This work is partly based on NUTS2 observations made with the NOT, operated by the NOT Scientific Association at the Observatorio

del Roque de los Muchachos, La Palma, Spain, of IAC. AL-FOSC is provided by IAA under a joint agreement with the University of Copenhagen and NOTSA. NUTS2 is funded in part by the Instrument Center for Danish Astrophysics (IDA). This work made use of ZTF data. We thank ZTF for access to this valuable public data stream and *Lasair* (<https://lasair.roe.ac.uk/>) which provides a broker system for users to access, visualise and extract science data

## REFERENCES

- Aguado D. S., et al., 2019, *ApJS*, 240, 23  
 Arnett W. D., 1982, *ApJ*, 253, 785  
 Asplund M., Grevesse N., Sauval A. J., Scott P., 2009, *ARA&A*, 47, 481  
 Branch D., Baron E., Thomas R. C., Kasen D., Li W., Filippenko A. V., 2004, *PASP*, 116, 903  
 Brown P. J., et al., 2009, *AJ*, 137, 4517  
 Cardelli J. A., Clayton G. C., Mathis J. S., 1989, *ApJ*, 345, 245  
 Chomiuk L., et al., 2016, *ApJ*, 821, 119  
 Chornock R., Filippenko A. V., Branch D., Foley R. J., Jha S., Li W., 2006, *PASP*, 118, 722  
 Dessart L., Hillier D. J., 2015, *MNRAS*, 447, 1370  
 Dopita M. A., Kewley L. J., Sutherland R. S., Nicholls D. C., 2016, *Ap&SS*, 361, 61  
 Filippenko A. V., Foley R. J., Silverman J. M., Chornock R., Li W., Blondin S., Matheson T., 2007, *CBET*, 926, 1  
 Fink M., et al., 2014, *MNRAS*, 438, 1762  
 Folatelli G., et al., 2012, *ApJ*, 745, 74  
 Foley R. J., et al., 2009, *AJ*, 138, 376  
 Foley R. J., et al., 2013, *ApJ*, 767, 57  
 Foley R. J., Jha S. W., Pan Y.-C., Zheng W. K., Bildsten L., Filippenko A. V., Kasen D., 2016, *MNRAS*, 461, 433  
 Fox O. D., et al., 2016, *ApJL*, 816, L13  
 Harutyunyan A. H., et al., 2008, *A&A*, 488, 383  
 Huchtmeier W. K., Petrosian A., Gopal-Krishna, McLean B., Kunth D., 2008, *A&A*, 492, 367  
 Jacobson-Galán W. V., et al., 2019, *MNRAS*, 487, 2538  
 Jha S., et al., 2006, *AJ*, 132, 189  
 Jha S. W., 2017, *hsn..book*, 375, *hsn..book*  
 Jordan G. C., Perets H. B., Fisher R. T., van Rossum D. R., 2012, *ApJL*, 761, L23  
 Kashyap R., Haque T., Lorén-Aguilar P., García-Berro E., Fisher R., 2018, *ApJ*, 869, 140  
 Kerzendorf W. E., Sim S. A., 2014, *MNRAS*, 440, 38  
 Kromer M., et al., 2013, *MNRAS*, 429, 2287  
 Kromer M., et al., 2015, *MNRAS*, 450, 3045  
 Kulkarni S. R., 2018, *ATel*, 11266, 1  
 Leloudas G., et al., 2019, *TNSAN*, 25, 1  
 Li W., et al., 2003, *PASP*, 115, 453  
 Liu W.-M., Chen W.-C., Wang B., Han Z. W., 2010, *A&A*, 523, A3  
 Lyman J. D., Taddia, F., Stritzinger, M., et al., 2018, *MNRAS*, 473, 1359  
 Lundqvist P. et al., 2020, *arXiv*, arXiv:2001.06070  
 Magee M. R., Sim S. A., Kotak R., Maguire K., Boyle A., 2019, *A&A*, 622, A102  
 Marino R. A., et al., 2013, *A&A*, 559, A114  
 McCully C., et al., 2014, *Natur*, 512, 54  
 Moriya T., et al., 2010, *ApJ*, 719, 1445  
 Moriya T. J., Eldridge J. J., 2016, *MNRAS*, 461, 2155  
 Mould J. R., et al., 2000, *ApJ*, 529, 786  
 Nomoto K., Kamiya Y., Nakasato N., 2013, *IAUS*, 253, IAUS..281  
 Parrent J. T., et al., 2011, *ApJ*, 732, 30  
 Perez-Torres M., et al., 2019, *ATel*, 13105, 1  
 Pettini M., Pagel B. E. J., 2004, *MNRAS*, 348, L59

- Phillips M. M., 1993, *ApJL*, 413, L105  
Phillips M. M., et al., 2007, *PASP*, 119, 360  
Piro A. L., Nakar E., 2014, *ApJ*, 784, 85  
Raddi R., et al., 2019, *MNRAS*, 489, 1489  
Riess A. G., et al., 1999, *AJ*, 118, 2675  
Riess A. G., et al., 2016, *ApJ*, 826, 56  
Sahu D. K., et al., 2008, *ApJ*, 680, 580  
Schlafly E. F., Finkbeiner D. P., 2011, *ApJ*, 737, 103  
Smith K. W., et al., 2019, *RNAAS*, 3, 26  
Stritzinger M., Leibundgut B., 2005, *A&A*, 431, 423  
Stritzinger M. D., et al., 2014, *A&A*, 561, A146  
Stritzinger M. D., et al., 2015, *A&A*, 573, A2  
Taubenberger S., 2017, *hsn..book*, 317, *hsn..book*  
Thomas R. C., Nugent P. E., Meza J. C., 2011, *PASP*, 123, 237  
Tomasella L., et al., 2016, *MNRAS*, 459, 1018  
Tonry J. L., 2011, *PASP*, 123, 58  
Valenti S., et al., 2009, *Natur*, 459, 674  
Vennes S., Nemeth P., Kawka A., Thorstensen J. R., Khalack V.,  
Ferrario L., Alper E. H., 2017, *Sci*, 357, 680

This paper has been typeset from a  $\text{\TeX}/\text{\LaTeX}$  file prepared by the author.